

A Statistical Study on Property of Spatial Magnetic Field for Solar Active Region

S. Liu¹

Received _____; accepted _____

Not to appear in Nonlearned J., 45.

¹Key Laboratory of Solar Activity, National Astronomical Observatories, Chinese Academy of Science, Beijing 100012, China

ABSTRACT

Magnetic fields dominate most solar activities, there exist direct relations between solar flare and the distributions of magnetic field, and also its corresponding magnetic energy. In this paper, the statistical results about the relationships between the spatial magnetic field and solar flare are given basing on vector magnetic field observed by the Solar Magnetic Field Telescope (SMFT) at Huairou Solar Observing Station (HSOS). The spatial magnetic fields are obtained by extrapolated photosphere vector magnetic field observed by SMFT. There are 23 active regions with flare eruption are chosen as data samples, which were observed from 1997 to 2007. The results are as follows: 1. Magnetic field lines become lower after flare for 16(69%) active regions; 2. The free energy are decreased after flare for 17 (74%) active regions. It can conclude that for most active regions the changes of magnetic field after solar flare are coincident with the previous observations and studies.

Subject headings: Magnetic Field, Flare, Corona

1. INTRODUCTION

Most solar activities such as filaments eruptions, flares and coronal mass ejections (CMEs) are dominated by magnetic fields. All these eruptions phenomena are energetic events due to explosive release of magnetic field energy (Krall et al. 1982; Shibata et al. 1995; Wang 1994; Tsuneta 1996; Forbes 2000; Bond et al. 2001; Priest & Forbes 2003; Nindos 2012). The magnetic field distributions and magnetic energies contained in active regions play the key roles in producing solar flares. Hence, the knowledge of magnetic field is necessary to understand solar activities (Valori et al. 2005; Wiegmann & Sakurai 2012). Previous researchers have studied lots of magnetic parameters related to the productions of flares, such as the magnetic flux of the active region (McIntosh 1990), the shear angle (Lv et al. 1993), the inductive electric field (Liu & Zhang 2008) and the magnetic helicity (Nindos & Zhang 2002, 2003). It is undoubted that there should exist changes of magnetic field before and after flares, since the sources of kinetic and thermal energy of flare are the magnetic energy release. The enhancements of transverse magnetic field were found after flare for some active regions (Wang et al. 2005; Su et al. 2012; Wang et al. 2012), which match the theoretical models (Hudson 2008, 2011; Li et al. 2011; Wang et al. 2012). More precisely, it is a fact that the flare energy comes from magnetic free energy, which is magnetic energy available in corona for conversion into kinetic and thermal energy (Regnier & Priest 2007). So the studies of relationships between free energy and flares may reveal more physical essences of flare productions. For example, Jing et al. (2009) found a positive correlation between the free energy and the flare index (Abramenko 2005), Sun et al. (2012) found there are evident decreases of free energy after the solar flares.

The whole spaces above the active regions are filled with magnetic fields, whose evolutions should be exhibited in whole spaces above active regions. However the magnetic fields with sufficient resolution and accuracy usually be measured on the photosphere, while magnetic field measurements in chromosphere and corona are only available for a few special cases (Solanki et al.

2003; Lin et al. 2004; Van Doorsselaere et al. 2008). To study the properties of spatial magnetic fields, the magnetic field extrapolations should be applied actually. Force free extrapolation is an classical method used to study solar spatial magnetic field recently. Force free extrapolations are based on the assumption that there is no Lorentz force in the whole space of active region, which can be expressed by $(\nabla \times \mathbf{B}) \times \mathbf{B} = 0$ mathematically. The spatial/coronal magnetic fields can be reconstructed from this physical model (namely, force free model: $(\nabla \times \mathbf{B}) \times \mathbf{B} = 0, \nabla \cdot \mathbf{B} = 0$), in which the observed photospheric magnetic fields are taken as a boundary conditions (Wu et al. 1990; Mikic et al. 1994; Amari et al. 1997; Sakurai 1981; Yan & Sakurai 2000; Wheatland et al. 2000; Wiegmann 2004; Song et al. 2006; He & Wang 2008; Liu et al. 2011a,b). It means that coronal magnetic fields are considered to be force free, while at the boundary it is connected to the photospheric magnetic fields observed.

In this paper, force free extrapolation (Song et al. 2006; Liu et al. 2011b) is used to obtained spatial magnetic field of active region, then the properties of magnetic field topology and free magnetic energy are studied. The main researches are targeted at the changes of magnetic field topology and free magnetic energy before and after solar flares, and the results are gained by large sample statistically. The remainder of this paper is organized as follows. In Section 2 the data and extrapolation method used are presented. In Section 3 the results are shown. At last, the discussions and conclusions are given in Section 4.

2. OBSERVATIONS DATA AND EXTRAPOLATION METHOD

The photosphere magnetograms used as boundary for extrapolation are observed by Solar Magnetic Field Telescope (SMFT) at Huairou Solar Observing Station (HSOS). SMFT consists of 35 cm refractor with a vacuum tube, birefringent filter, CCD camera including an image processing system (Ai & Hu 1986). The birefringent filter is tunable, working either at the photosphere line Fe I λ 5324.19 Å, with a 0.150 Å bandpass, or at the chromosphere line, H β ,

with a 0.125 Å bandpass. The line of Fe I λ 5324.19 Å (Lande factor $g = 1.5$) formed around the solar photosphere, is used for photospheric magnetic field observations. The bandpass of the birefringent filter is about 0.15 Å for Fe I λ 5324.19 Å line. The center wavelength of the filter can normally be shifted -0.075 Å relative to center of Fe I λ 5324.19 Å to measure of the longitudinal magnetic field and then the line center is applied to measure the transverse one (Ai & Hu 1986). Vector magnetograms are reconstructed from four narrow-band images of Stokes parameters (I , Q , U and V). V is the difference of the left and right circularly polarized images, Q and U are the differences between two orthogonal linearly polarized images for different azimuthal directions, I is the intensity derived from either the sum of two circularly polarized images is the line-of-sight field measurements or of two linearly polarized images in the transverse field measurement. When I , Q , U and V are measured, the corresponding white light images are simultaneously obtained, which are employed to compensate for the time differences during the measurements of I , Q , U and V . The sequence of obtaining Stokes images is as follows: First acquired the V/I image ; next the Q/I images, then the U/I image. The time required to obtain a set of Stokes images was about 45 seconds. Each image is associated with 256 integrated frames. To reconstruct the vector magnetograms, the linear relation is necessary between the magnetic field and the Stokes parameters I , Q , U and V , which is true under the weak-field approximation (Jefferies et al. 1989; Jefferies & Mickey 1991):

$$B_L = C_L V, \quad (1)$$

$$B_T = C_T (Q^2 + U^2)^{1/4}, \quad (2)$$

$$\theta = \arctan\left(\frac{B_L}{B_\perp}\right), \quad (3)$$

$$\phi = \frac{1}{2} \arctan\left(\frac{U}{Q}\right), \quad (4)$$

where B_L and B_T are the line-of-sight and transverse component of the photospheric field, respectively. θ is the inclination between the vector magnetic field and the direction normal to the solar surface and ϕ is the field azimuth. C_L and C_T are the calibration coefficients for

the longitudinal and transverse magnetic fields, respectively. In this study, C_L and C_T are 8381 G and 6790 G (Wang, Ai & Deng 1996; Su & Zhang 2004), respectively, which are obtained by theoretical calibration. After routine data processing of HSOS data, the spatial resolution of observational data is actually 2 arcsec/pixel \times 2 arcse/pixel and 3σ noise levels of vector magnetograms are 20 G and 150 G for longitudinal and transverse components, respectively. To resolve 180° ambiguity, the method of minimum energy are employed, this method minimizes simultaneously both the divergence of the magnetic field ($\nabla \cdot \mathbf{B}$) and the electric current density ($\mathbf{J} = \nabla \times \mathbf{B}$) using a simulated annealing algorithm (Metcalf 1994; Metcalf et al. 2006). At last, the components of the vector magnetic field projected and re-mapped to local heliographic coordinates are used for magnetic field extrapolation.

The approximate vertical integration (AVI) method (Song et al. 2006) was improved from the direct integration method (Wu et al. 1990) basing on equations (5)-(8).

$$\frac{\partial B_x}{\partial z} = \frac{\partial B_z}{\partial x} + \alpha B_y, \quad (5)$$

$$\frac{\partial B_y}{\partial z} = \frac{\partial B_z}{\partial y} - \alpha B_x, \quad (6)$$

$$\frac{\partial B_z}{\partial z} = -\frac{\partial B_x}{\partial x} - \frac{\partial B_y}{\partial y}, \quad (7)$$

$$\alpha B_z = \frac{\partial B_y}{\partial x} - \frac{\partial B_x}{\partial y}. \quad (8)$$

The magnetic field is reconstructed by the following formula firstly in AVI method,

$$\mathbf{B}_x = \xi_1(x, y, z)F_1(x, y, z), \quad (9)$$

$$\mathbf{B}_y = \xi_2(x, y, z)F_2(x, y, z), \quad (10)$$

$$\mathbf{B}_z = \xi_3(x, y, z)F_3(x, y, z), \quad (11)$$

assuming the second-order continuous partial derivatives in a certain height range, $0 < z < H$ (H is the height from the photosphere). In Equations (9)-(11), ξ_1, ξ_2 and ξ_3 mainly depend on z

and slowly vary with x and y , while F_1, F_2 and F_3 mainly depend on x and y and weakly vary with z , which are mathematical representation of the similarity solutions. In solar active regions, we cannot seek analytical solutions for the magnetic field, but we can construct an analytical asymptotic solutions within a thin layer.

After constructing the magnetic field, the following integration equations,

$$\begin{aligned}
 \frac{d\xi_1}{dz}F_1(x_i, y_j, z) &= \xi_3 \frac{\partial F_3(x_i, y_j, z)}{\partial x} + \alpha(x_i, y_j, z)\xi_2 F_2(x_i, y_j, z), \\
 \frac{d\xi_2}{dz}F_2(x_i, y_j, z) &= \xi_3 \frac{\partial F_3(x_i, y_j, z)}{\partial y} - \alpha(x_i, y_j, z)\xi_1 F_1(x_i, y_j, z), \\
 \frac{d\xi_3}{dz}F_3(x_i, y_j, z) &= -\xi_1 \frac{\partial F_1(x_i, y_j, z)}{\partial x} - \xi_2 \frac{\partial F_2(x_i, y_j, z)}{\partial y}, \\
 \alpha(x_i, y_j, z)\xi_3 F_3(x_i, y_j, z) &= \xi_2 \frac{\partial F_2(x_i, y_j, z)}{\partial x} - \xi_1 \frac{\partial F_1(x_i, y_j, z)}{\partial y},
 \end{aligned} \tag{12}$$

for $0 \leq z \leq \Delta z$.

are used to carry out the extrapolation. The solutions of the above equations can be found in Song et al. (2006). The performances of this AVI extrapolation method are evaluated in some previous studies. Through the related investigations and comparisons, it is concluded that this method is acceptable for corona magnetic field extrapolation (Song et al. 2006, 2007; Liu et al. 2011a,b). Also there are some actual applications about this AVI extrapolation to study the chromosphere and corona magnetic field (Song et al. 2007; Li et al. 2011a; Liu et al. 2011b).

3. RESULTS

In this work 23 active regions with flare eruptions observed by SMFT from 1997 to 2007 are selected as data sample. The criteria of the selection for active regions are as follows: 1. The magnetic fields were obtained at a time interval of ~ 3 hours before and after solar flare, it means

that there are individual observation before and after flare, and the time differences between flare and observations should not be longer than 3 hours. 2. The solar flare should be a single one, it requires that there must be only one flare within the observations time interval of before and after this flare, there should be no redundant flare occurring during this time interval. 3. The magnetic components of B_x , B_y and B_z can be reconstructed normally and completely, there should be no observation data with defects are used in the work. 4. The longitudes of active regions observed and used for study should locate within 40 degree away from solar disk center. 5. The deviations of magnetic fluxes between positive and negative magnetic field should not exceed 20%, which can be express by formula $(F_p - F_n)/F_p \leq 20\%$ (F_p and F_n indicate positive and negative magnetic fluxes, respectively). Through a rigorous selection, 23 active regions selected and listed in Table 1 are chosen for this study. In the table, the number of active region (NOAA), the observation time, the flare eruption time, the flare level and the deviation of flux are given.

The extrapolated fields should represent the solutions of force-free equations ($(\nabla \times \mathbf{B}) \times \mathbf{B} = 0$, $\nabla \cdot \mathbf{B} = 0$) approximately, so the extent of force- and divergence-freeness of extrapolated field should be checked at first. The criterion of force-freeness σ_J ,

$$\sigma_J = \frac{\sum_i J_i \sigma_i}{\sum_i J_i}, \quad (13)$$

where

$$\sigma_i = \sin \theta_i = \frac{|\mathbf{J} \times \mathbf{B}|_i}{J_i B_i}, \quad (14)$$

and the criterion of divergence-freeness f_i ,

$$f_i = \frac{\int_{\Delta S_i} \mathbf{B} \cdot d\mathbf{S}}{\int_{\Delta S_i} |\mathbf{B}| d\mathbf{S}} \approx \frac{(\nabla \cdot \mathbf{B})_i \Delta V_i}{B_i A_i}, \quad (15)$$

are used to check the quality of the extrapolated field (Wheatland et al. 2000; DeRosa et al. 2009). σ_J are the weighted average of the sine of angle between the magnetic field and current density, and it is related to Lorentz force. The average magnitude of f_i is used to assess the divergence free. Where A_i is the surface area of the differential volume (ΔV_i). σ_J and $\langle |f_i| \rangle$ should be equal

to zero, when the force- and divergence-freeness of extrapolated field are fully satisfied. Fig1 gives the distributions of σ_J and $\langle |f_i| \rangle$ for these 23 active regions. And for each criterion, the corresponding mean values are given in this figure. It can be found that the σ_J ranges from 0.21 (Rad) to 0.76 (Rad) with mean values 0.40 (Rad), while $\langle |f_i| \rangle$ ranges from 0.13×10^{-4} to 0.83×10^{-4} with mean values 0.49×10^{-4} . The amplitudes of σ_J and $\langle |f_i| \rangle$ are comparable to the previous studies (Liu et al. 2011a; Wheatland et al. 2000). Another aspect to assess the quality of extrapolated field can be done by comparisons of magnetic field lines with coronal images. To see the consistences between field lines and coronal loops, here three examples are given in Fig2, 3 and 4, respectively. Here the left panel shows the magnetic field lines which are over plotted on the EIT/SOHO image, and the pure coronal image are given in right panel to see the coronal image clearly. It can be seen that the magnetic field lines can match coronal loops for global structures at some extent, especially for closed field lines (red lines plotted in left panels). On the whole the extrapolated field for these active regions approximately satisfy conditions of force-free equations since the criterion of force-freeness and divergence-freeness are acceptable at some extent, and the extrapolated field lines can match coronal loops for global structures. So it is reasonable to tentatively study the properties of spatial magnetic fields for these active regions using the extrapolated fields.

Fig5 shows the changes amplitudes of magnetic components of B_x , B_y , B_z , B_t and the inclination angle, which is defined by $\text{atan}(B_t/B_z)$, B_t is the transverse magnetic field ($B_t = \sqrt{B_x^2 + B_y^2}$). For each component, its differences between corresponding values after and before flare are normalized to its values after flare. So the positive/negative values mean the increases/decreases of this component after the occurrences of flares, and the values indicate the relative rates of increases after solar flares. As for the inclinations angles, here only closed field lines are calculated and averaged to avoid the biased that may originate from open field lines. For the value of each individual component, it is calculated from the magnetic fields amplitudes of the whole space of active region. For example, $B_x = (1/N) \sum < |B_x(i, j, k)| >$ (i, j and k is the

pixel position of 3D space, N is the total number of vectors in the volume to be calculated) is the average of absolute values of magnetic fields. In this figure, the plots of a, b, c, d and e correspond to the components of B_x , B_y , B_z , B_t and the inclination angle, respectively. The changes of those magnetic components can indicate the topology changes of space magnetic fields, hence they are chosen to be studied firstly. For example, the increases of transverse magnetic field can mean that magnetic field lines become more lower after flare than those before solar flare. Also the increases/decreases of inclination angles indicate most evidently that magnetic field lines become lower/higher after solar flare. In figure 1, it can be found that the number of active with the increases of B_x , B_y , B_z , B_t and inclination angle are 16, 15, 8, 16 and 16, respectively. It is found that the change amplitudes of B_x , B_y , B_z , B_t do not exceed 20%, but the change amplitudes of inclination angle exceed 20% for a few active regions. Through the distributions of inclination angles it can be found that there are 69% (16/23) active region with field line lower after flare. In this figure, the plot of f, g, h and i shows the correlations between inclination angle and B_x , B_y , B_z , B_t . It can be found that there are positive correlations between the inclination angle and B_x , B_y , B_t , the correlation coefficients are 97%, 89% and 94% between the inclination angle and B_x , B_y , B_t , respectively. There is weak negative correlations between the inclination angles and B_z with correlation coefficient of 71%.

It is considered traditionally that free magnetic energy is more related to solar flare. The free magnetic energy is the energy difference between actual magnetic field and the corresponding potential field (the minimum energy state for a given photosphere boundary condition). In the practical application, free magnetic energy can be calculated by the following formula:

$$E_{free} = E_N - E_P = \int \frac{B_N^2}{2\mu} dV - \int \frac{B_P^2}{2\mu} dV \quad (16)$$

where V is the computational volume from photosphere to corona, and the superscripts N and P represent the non-linear force free field (approximate actual space magnetic field of active region) and the potential field, respectively. Fig6 shows the changes of free energy of those active regions.

Same as Fig5, the differences of free energy between after and before flare are normalized to its values after flare. Also, the positive/negative values mean the increase/decrease of free energy of corresponding active region. From plot a, it can be found that there are 74% (17/23) active regions with free energy decrease after solar flare. In plot b, the correlations between changes of free energy and inclination angle are shown, it can be found that there exist weak negative correlations with correlation coefficient of 66%. Additionally, for 6 active regions with free energy increase, there are 3 active regions with inclination decrease. While for 17 active regions with free energy decrease, there are only 4 active regions with inclination angle decrease.

4. DISCUSSIONS AND CONCLUSIONS

In this work, the statistical researches on the properties of space magnetic field before and after solar flare are presented basing on observations obtained by SMFT installed at HSOS. The regularization of magnetic topology indicated partially by the changes of inclination angle can display the evolutions of active region spatial magnetic fields. While free magnetic energy is related the most profound physical essence, which can explicate the productions of solar flare undoubtedly, due to solar flare energy come from free magnetic energy. So the main studies are focused on the changes of inclination angles and free magnetic energy before and after solar flare in this research.

The selection criteria described in the above section for active regions with flare eruption are very rigorous in this study, since the precise changes of magnetic field after solar flare are the primary focuses, at last 23 active regions are chosen as data sample in this study. Through calculations, it is found that 16 (69%) active regions with inclination angle increases, it is means that the transverse fields increase relatively after solar flare, which can match the previous theoretical model (Hudson 2008, 2011). For free magnetic energy, there are 17 (74%) active regions with the decreases of free energy, which are similar to some previous research results

(Sun et al. 2012). It is noted for the changes of free magnetic energy that changes amplitudes of free energy decreases are larger than those of free energy increases. Similarly, the changes amplitudes of inclination angle increases are larger than those of inclination angle decreases.

In this paper, the sensitive magnetic parameters related to the productions of solar flare are calculated from the observations. It can not give the exact conclusions which parameter is direct related to solar flare. However, it can be concluded that the results of most active regions agree with the previous studies, which have given the conclusions that the transverse magnetic field (free magnetic energy) will increase (decrease) after the eruption of solar flare. For active regions not match the classical theoretical model, there maybe some more complicated factors that lead to the corresponding results. Additionally, it is should noted that there are some uncertainties on observation data and numerical extrapolation, which all can affect the precise of statistical results.

This work was partly supported by the Grants: 2011CB811401, KLCX2-YW-T04, KJCX2-EW-T07, 11203036, 11221063, 11178005, 11003025, 11103037, 11103038, 10673016, 10778723 and 11178016, the Young Researcher Grant of National Astronomical Observations, Chinese Academy of Sciences, and the Key Laboratory of Solar Activity National Astronomical Observations, Chinese Academy of Sciences.

Table 1: The active regions selected.

NOAA	Date	Observation Time	Flare Time	Observation Time	Flare	Flux Deviation
		Before Flare	(UT)	After Flare (UT)	Level	$(F_p - F_n)/F_p$ Before—After
08040	1997-05-21	04:13:21	06:04	06:18:21	C _{2.7}	12%—15%
08156	1998-02-15	03:26:03	04:20	04:58:49	C _{1.8}	15%—16%
08218	1998-05-12	00:21:58	04:49	07:07:51	C _{1.2}	17%—16%
08319	1998-08-28	23:07:55	00:36	01:48:13	C _{1.2}	16%—14%
08369	1998-10-28	01:43:09	02:03	02:21:44	C _{1.6}	13%—9%
08716	1999-10-07	04:21:36	05:19	06:32:08	C _{2.2}	12%—10%
08728	1999-10-16	04:32:18	05:05	06:31:26	C _{2.3}	8%—11%
08737	1999-10-21	04:31:49	06:20	06:40:21	C _{1.9}	15%—12%
08925	2000-03-30	04:32:18	05:05	06:31:26	C _{2.3}	11%—10%
09054	2000-06-16	05:16:59	06:31	07:03:40	C _{3.2}	17%—12%
09154	2000-09-06	02:25:45	03:38	04:04:07	C _{1.7}	9%—14%
09321	2001-06-16	05:40:01	07:08	07:52:06	C _{1.0}	12%—10%
09463	2001-05-25	23:02:45	23:57	03:28:32	C _{1.7}	10%—11%
09531	2001-07-11	00:20:17	00:41	01:34:35	C _{1.0}	13%—15%
10061	2002-08-09	04:37:43	06:36	06:48:31	C _{1.4}	12%—9%
10119	2002-09-20	01:07:31	01:56	03:55:21	C _{2.4}	6%—8%
10137	2002-10-03	01:25:53	02:15	03:00:06	M _{2.1}	7%—9%
10488	2003-10-27	23:50:30	00:41	01:14:24	C _{5.3}	9%—11%
10767	2005-05-27	04:31:00	05:00	05:25:38	C _{2.5}	13%—11%
10786	2005-07-05	01:11:46	01:24	01:48:02	M _{1.8}	14%—11%
10826	2005-12-03	05:06:01	05:31	06:06:42	M _{3.6}	12%—13%
10953	2007-5-02	23:27:54	23:28	00:03:26	C _{8.5}	14%—12%
10960	2007-06-05	03:48:36	04:15	04:31:49	C _{1.2}	15%—17%

REFERENCES

- Abramenko, V.I.: 2005, *ApJ*, **629**, 1141
- Ai, G. & Hu, Y.: 1986, *Acta Astron. Sinica*, **27**, 173,
- Amari, T., Aly, J.J., Luciani, J.F., Boulmezaoud, T.Z., Mikic, Z.: 1997, *Sol. Phys.* **174**, 129.
- Bond, H. E., Mullan, D. J., O’Brien, M. S., & Sion, E. M.: 2001, *ApJ* **560**, 919
- DeRosa, M.L., Schrijver, C.J., Barnes, G., Leka, K.D., Lites, B.W., Aschwanden, M.J., Amari, T., Canou, A., McTiernan, J.M., Rgnier, S., Thalmann, J.K., Valori, G., Wheatland, M.S., Wiegmann, T., Cheung, Mark C.M., Conlon, P.A., Fuhrmann, M., Inhester, B., & Tadesse, T.: 2009, *ApJ* **696**, 1780
- Forbes, T.G.: 2000, *J. Geophys. Res.*, **105**, 23153
- He, H., Wang, H.: 2008, *J. Geophys. Res.* **113**, A05S90
- Hudson, H.S., Fisher, G.H., Welsch, B.T.: 2008, in *ASP Conf. Ser. 383 Subsurface and Atmospheric Influences on Solar Activity*, ed. R. Howe et al. (San Francisco, CA: ASP), 221
- Hudson, H.S.: 2011, *Space Sci. Rev.*, **7**, 5
- Jefferies, J., Lites, B.W. & Skumanich, A.: 1989, *ApJ* **343**, 920
- Jefferies, J., & Mickey, D.L.: 1991, *ApJ* **372**, 694
- Jing, J., Tan, C.Y., Yuan, Y., Wang, B., Wiegmann, T., Xu, Y. & Wang, H.M.: 2009, *ApJ*, **713**, 440
- Krall, K. R., Smith, J. B., Jr., Hagyard, M. J., West, E. A. & Cummings, N. P.: 1982, *Sol. Phys.* **79**, 59

- Li, H., Schmieder, B., Song, M.T., & Bommier, V.: 2007, A&A **475**, 1081
- Li, Y., Jing, J., Fan, Y., Wang, H.M.: 2011, ApJ **727**, L19
- Lin, H., Kuhn, J. R. & Coulter, R.: 2004, ApJ **613**, L17789
- Liu,S., Zhang, H.Q. & Su, J.T.: 2011, Sol. Phys. **270**, 89
- Liu,S., Zhang, H.Q., Su, J.T. & Song, M.T.: 2011, Sol. Phys. **269**, 41
- Liu, J.H. & Zhang, H.Q.: 2008, Advances in Space Research., **39**, 1835
- Lv, Y.P., Wang, J.X.: 1993, Sol. Phys. **1485**, 119
- McIntosh, Patrick S.: 1990, Sol. Phys. **125**, 251
- Metcalf, T. R.: 1994, Sol. Phys. **155**, 235.
- Metcalf, T. R., Leka, K. D., Barnes, G., Lites, B. W., Georgoulis, M. K., Pevtsov, A. A., Balasubramaniam, K. S., Gary, G. A., Jing, J., & Li, J.: 2006, Sol. Phys. **237**, 267.
- Mikic, Z.; McClymont, A. N.: 1994, in Solar Active Region Evolution: Comparing Models with Observations, Vol68. ASP Conf. Ser., p.225.
- Nindos, A. & Zhang, H.Q.: 2002, ApJ **573**, L133
- Nindos, A., Patsourakos, S. & Wiegmann, T. 2012, ApJ, **748**, L6
- Nindos, A. & Zhang, H.Q.: 2003, ApJ **594**, 1033
- Priest, E.R. & Forbes, T.G.: 2002, *Astron. Astrophys. Rev.* **10**, 313
- Regnier, S. & Priest, E.R.: 2007, A&A **669**, L53
- Wang T.J., Ai G.X., Deng, Y.Y.: 1996, *Astrophysics Reports*., **23**, 31

- Sakurai, T.: 1981, *Sol. Phys.* **69**, 343.
- Shibata, K., S. Masuda, M. Shimojo, H. Hara, T. Yokoyama, S. Tsuneta, T. Kosugi, & Y. Ogawara: 1995, *ApJ* **451**, L83
- Su, J.T. & Zhang, H.Q.: 2004, *Chin. J. Astron. Astrophys.* **4**, 365
- Su, J.T., Jing, J., Wang, H. M., Mao, X. J., Wang, X. F., Zhang, H. Q., Deng, Y. Y., Guo, J., Wang, G.P., 2011, *ApJ* **733**, 94
- Solanki, S.K., Lagg, A., Woch, J., Krupp, N. & Collados, M.: 2003, *Nature* **425**, 692
- Song, M.T., Fang, C., Tang, Y.H., Wu, S.T., Zhang, Y.A.: 2006, *ApJ* **649**, 1084.
- Song, M.T., Fang, C., Zhang, H.Q., Tang, Y.H., Wu, S.T., Zhang, Y.A.: 2007, *ApJ* **666**, 491.
- Sun, X.D., Hoeksema, J.T., Liu, Y., Wiegelmann, T., Hayashi, K., Chen, Q.R. & Thalmann, J.: 2012, *ApJ*, **748**, 77
- Tsuneta, S.: 1996, *ApJ* **456**, 840
- Valori, G., Kliem, B., Keppens, R.: 2008, *A&A* **433**, 335
- Van Doorselaere, T., Nakariakov, V. M., Young, P. R. & Verwichte, E.: 2008, *A&A* **487**, L17
- Wang, H., Ewell, M. W., Jr., Zirin, H. & Ai, G.X.: 1994, *ApJ* **424**, 436.
- Wang, H.M., Liu, C., Deng, Y.Y., Zhang, H.Q.: 2005, *ApJ* **627**, 1031
- Wang, H.M., Liu, C., Liu, R., Deng, N., Liu, Y., Wang, H.M.: 2012, *ApJ* **745**, L17
- Wheatland, M.S., Sturrock, P.A., Roumeliotis, G.: 2000, *ApJ* **540**, 1150.
- Wiegelmann, T.: 2004, *Sol. Phys.* **219**, 87.

Wiegmann, T., Sakurai, T.: 2012, *LivingRev. Sol. Phys.* **9**, 5.

<http://solarphysics.livingreviews.org/Articles/lrsp-2012-5/>

Wu, S.T., Sun, M.T., Chang, H.M., Hagyard, M.J., Gary, G.A.: 1990, *ApJ* **362**, 698.

Yan, Y., Sakurai, T.: 2000, *Sol. Phys.* **195**, 89.

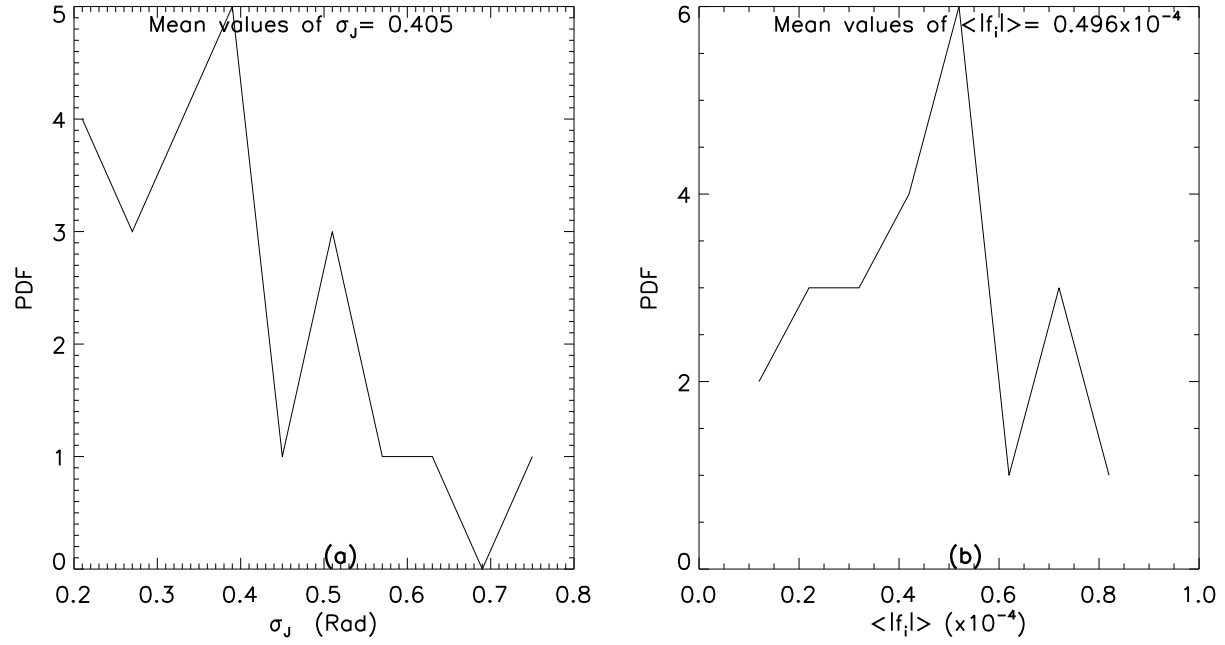


Fig. 1.— The distributions of σ_J and $\langle |f_i| \rangle$ for all active regions studied, and the corresponding mean values are given in each plot individually.

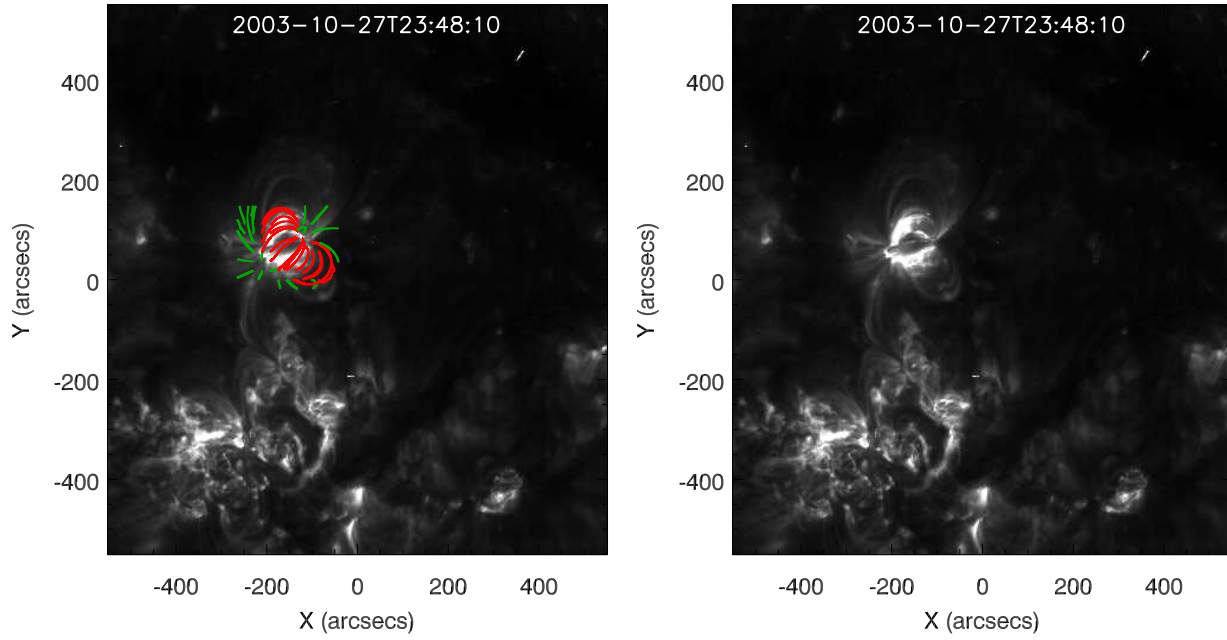


Fig. 2.— The left: the distributions of magnetic field lines are over plotted on the coronal images. The right: the coronal images obtained by EIT/MDI at 2003-10-27T23:48:10UT.

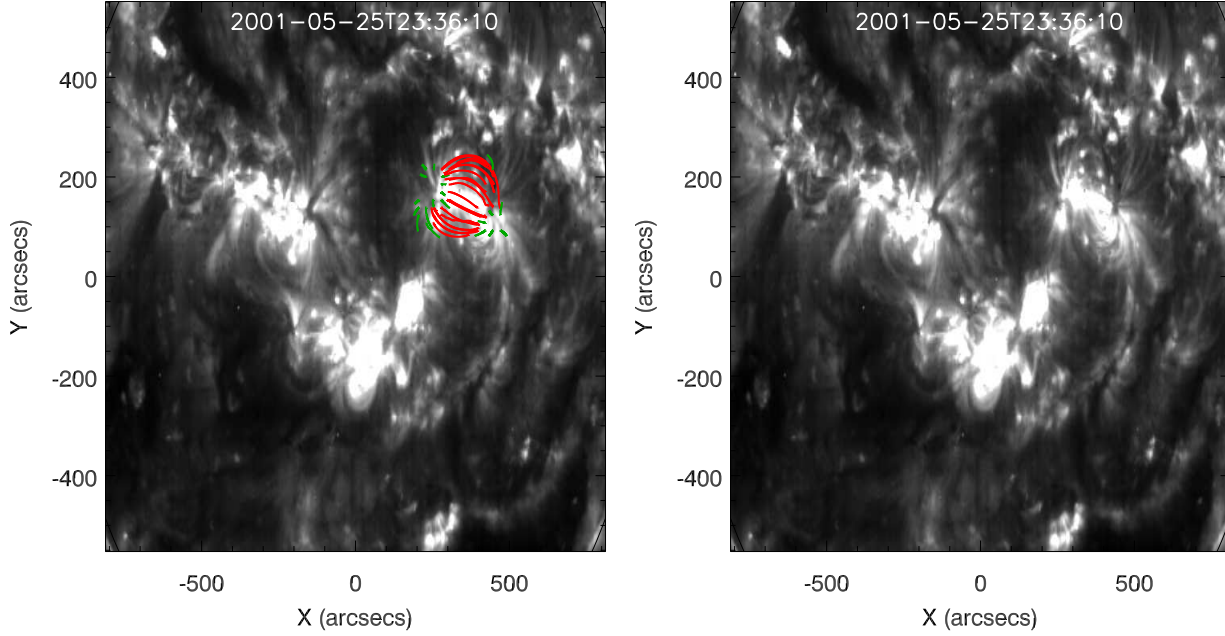


Fig. 3.— Same as Fig2, but the observed time is 2001-05-25T23:36:10UT.

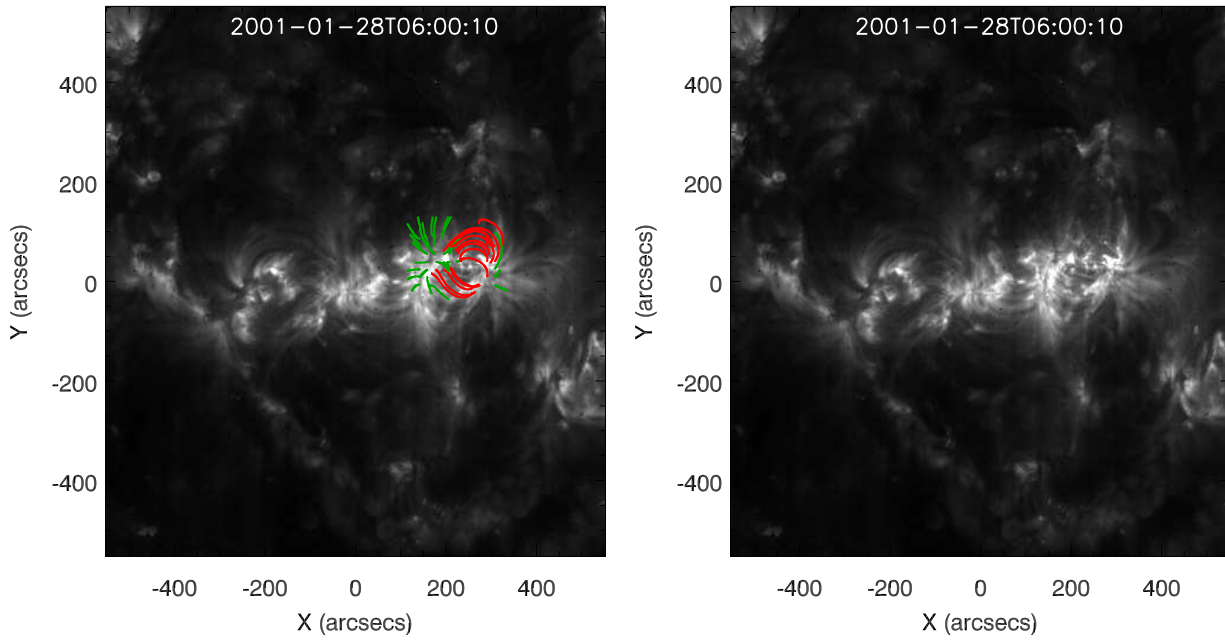


Fig. 4.— Same as Fig2, but the observed time is 2001-01-28T06:00:10UT.

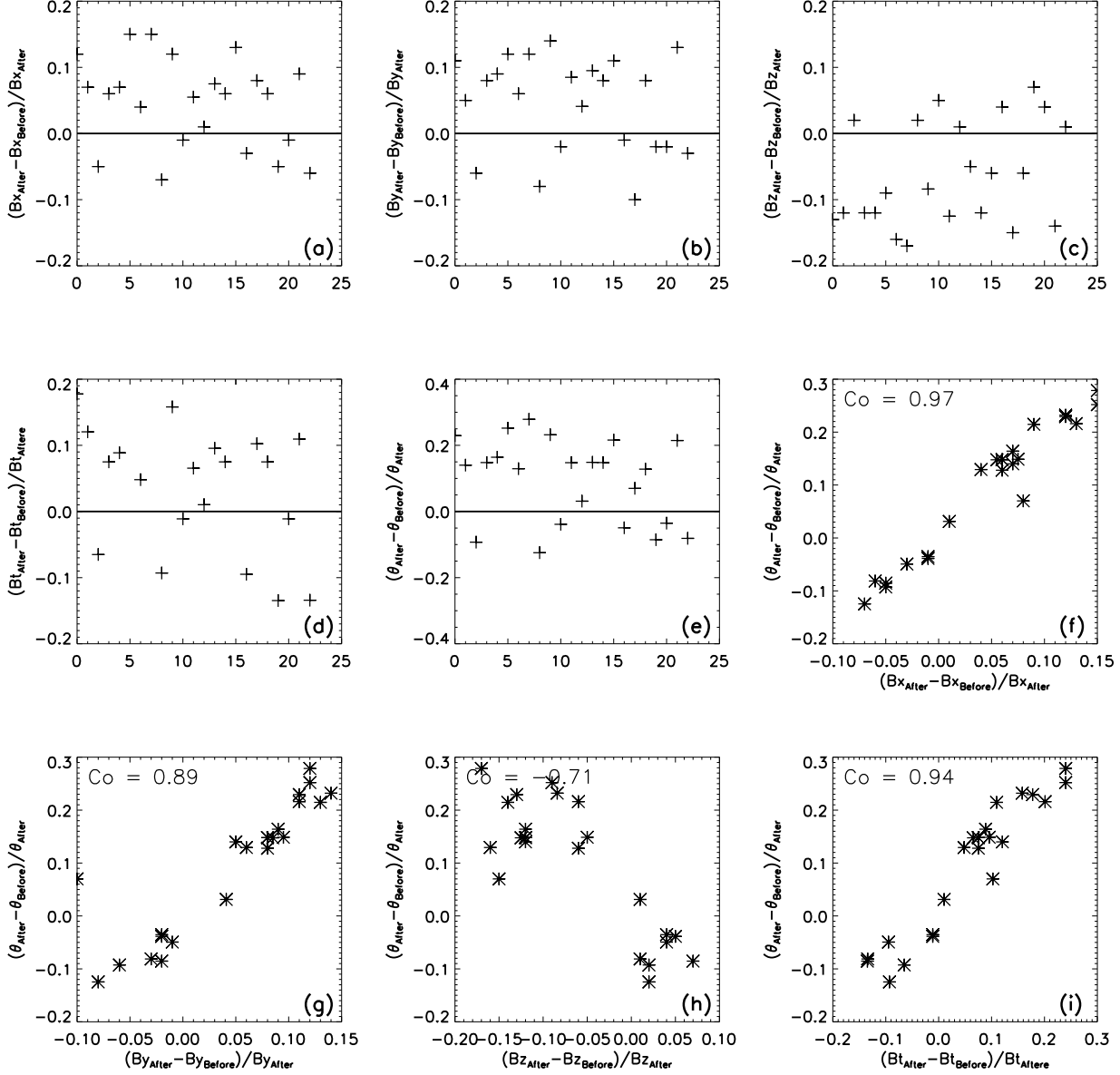


Fig. 5.— Plots of a, b, c, d and e show the changes of magnetic components of B_x , B_y , B_z , B_t and the inclination angle (θ), respectively. For each component, the differences of those component between after and before flare are normalized to its values after flare. Here inclinations angles are calculated and averaged basing on closed field lines. Plots of f, g, h and i show the correlations between the changes of B_x , B_y , B_z , B_t and the changes of inclination angle (θ), and the correlation coefficients are calculated and labeled on corresponding panels.

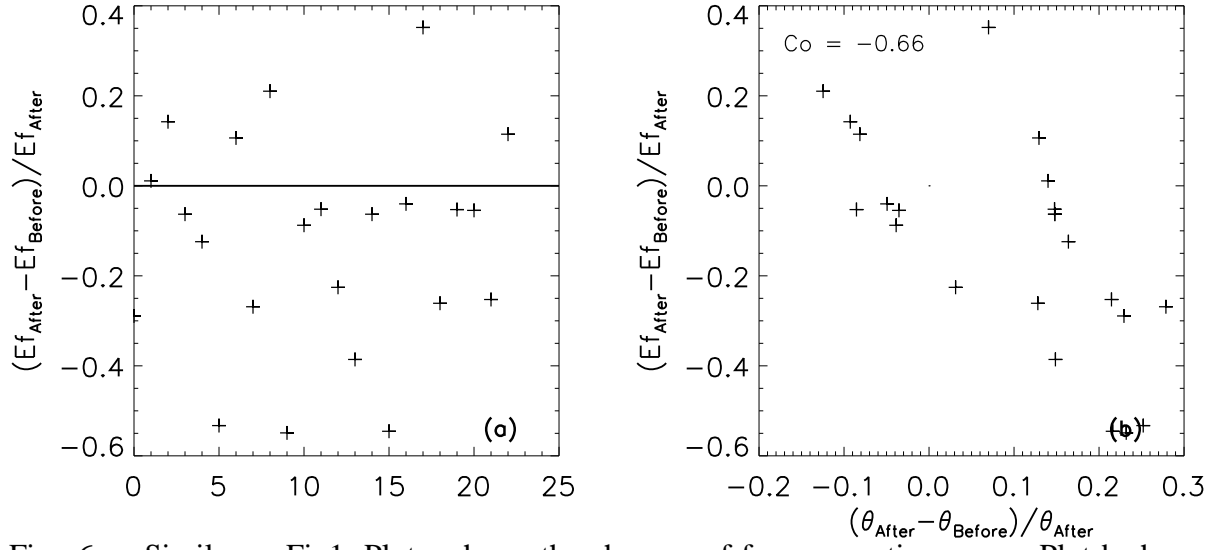


Fig. 6.— Similar as Fig1, Plot a shows the changes of free magnetic energy. Plot b shows the correlations between the changes of free energy and the changes of inclination angle (θ), and the correlation coefficient is calculated and labeled.